Journal of Alloys and Compounds 777 (2019) 775–783

Contents lists available at ScienceDirect

Journal of Alloys and Compounds

journal homepage: http://www.elsevier.com/locate/jalcom

SnSb alloy nanoparticles embedded in N-doped porous carbon nanofibers as a high-capacity anode material for lithium-ion batteries

Zhaoxia Yuan [a, b], Linxi Dong [a], Qili Gao [b], Zhenguo Huang [c], Luwen Wang [a, *], Gaofeng Wang [a, **], Xuebin Yu [a, b, ***]

[a] Key Laboratory of RF Circuits and System of Ministry of Education, Electronic and Information College of Hangzhou Dianzi University, Hangzhou 310018, China
[b] Department of Materials Science, Fudan University, Shanghai, China
[c] School of Civil and Environmental Engineering, University of Technology Sydney, Australia

ARTICLE INFO

Article history:
Received 6 September 2018
Received in revised form
22 October 2018
Accepted 23 October 2018
Available online 26 October 2018

Keywords:
N-doped porous carbon nanofibers
Lithium azide
SnSb alloy nanoparticles
Electrospinning
Lithium-ion batteries

ABSTRACT

SnSb alloy is a promising anode material for lithium-ion batteries due to its high specific capacity. However, the large volume change in the process of charge/discharge causes significant pulverizing of SnSb alloy particles, which leads to a rapid capacity fading. This paper reports the synthesis of homogenous SnSb nanoparticles that are embedded in N-doped porous carbon nanofibers through electrospinning technique with LiN_3 serving as poregen agent. This distinctive structure prevents the direct contact of SnSb nanoparticles with the electrolyte and provides enough space for the volume change of SnSb alloy during the Li^+ insertion/extraction process, enabling this material to deliver a high reversible capacity of 892 mA h g^{-1} after 100th cycle at 100 mA g^{-1}, and a stable capacity of 487 mA h g^{-1} after 1000 cycles at 2000 mA g^{-1}. These results highlight the importance of the synergistic effect of SnSb alloy nanoparticles and N-doped porous carbon nanofibers for the high performance of lithium-ion batteries.

1. Introduction

With the increasing consumption of nonrenewable fossil fuels, great efforts have been devoted to exploring alternative power sources for portable electronic devices and electric vehicles [1–6]. Due to its high energy density, long cycle time, and environment-friendly, rechargeable lithium-ion batteries are considered to be one of the most promising alternative power sources for these applications [7–10]. Although commercial graphite anode materials have good electrochemical performance, its low theoretical capacity (372 mA h g^{-1}) could not meet the increasing demand [11]. Therefore, it is necessary to seek alternative anode materials with enhanced capacity, stability and rate performance [12].

Sn-based material has been considered as a promising anode materials due to its high theoretical capacity (990 mA h g^{-1}) in LIBs [13–15]. However, a serious problem suffered in this system is that the Sn-based material has a relatively large volume change (up to 300%) during repeated charge-discharge process, which will cause the pulverizing and crack of the material, and affect its rate performance and cycling life in the practical application [16]. Recently, Sn-based intermetallic alloys, such as Sn-Sb, Sn-Ni, Sn-Se alloy, and so forth, have been demonstrated to be effective to overcome these problems [17–19]. Specifically, SnSb alloy exhibits excellent lithium storage ability because both Sn and Sb have the capability to store lithium ions, which contributes to the entire specific capacity [20]. Since the lithiation/delithiation reaction of Sn and Sb occurs at different potentials, the inert phase may act as a buffer to accommodate volume expansion during the lithiation reaction [21,22]. As a result, the gradual lithium insertion mechanism can prohibit the volume expansion and improve mechanical stability of the electrode, ensuring SnSb alloy better electrochemical performance than a single Sn or Sb phase [23–25].

So far, a lot of research has been devoted to the synthesis of diverse SnSb alloy material to improve the electrochemical performance. It is found that to control the particle size in the nanometer range can effectively solve mechanical strain in the charge/

* Corresponding author.
** Corresponding author.
*** Corresponding author. Key Laboratory of RF Circuits and System of Ministry of Education, Electronic and Information College of Hangzhou Dianzi University, Hangzhou 310018, China.
E-mail addresses: wangluwen@hdu.edu.cn (L. Wang), gaofeng@hdu.edu.cn (G. Wang), yuxuebin@fudan.edu.cn (X. Yu).

https://doi.org/10.1016/j.jallcom.2018.10.295
0925-8388/

discharge process, decrease the distance between the ion and electron transport, and enhance the electrochemical performance [26–29]. However, the SnSb nanoparticles tend to agglomerate during the cycling process, and the solid electrolyte interface (SEI) film is repeatedly decomposed and formed, which deteriorates the cycle performance of the material [30,31]. According to previous reports, a variety of carbon materials, such as carbon nanotubes, carbon nanofibers, graphene nanocomposites and so on, have been developed as buffer matrix to mitigate the volume expansion [32,33]. Furthermore, it was found that the design and synthesis of porous carbon nanofibers coated SnSb nanoparticles can provide enough space to alleviate the volume expansion/contraction and particle agglomeration problems of SnSb alloys during repeated insertion/extraction of Li^+ [34–37]. Furthermore, the porous structure can also reduce the transport length of Li-ions and supply a large electrode/electrolyte interface for charge transfer reactions, effectively improving the electrochemical performance of the anode materials [38,39]. However, it is still a challenge to create carbon nanofibers with a uniformly distributed porous structure to in-situ decorate the SnSb nanoparticles [40,41].

In this work, we propose a simple and inexpensive method through an electrospinning strategy and subsequent heat treatment to fabricate N-doped porous carbon nanofibers embedded SnSb nanoparticles (SnSb@N-PCNFs) as anode material for LIBs. By employing lithium azide as a porogen, during the carbonization process, lithium azide reacts with nitrogen to strongly release nitrogen, resulting in a strong repulsive force that can lead to the formation of a homogeneous, completely porous carbon nanofiber. Furthermore, the lithium azide can also play a role of nitrogen source, thereby realizing the formation of N-doped porous carbon nanofibers. Nitrogen atoms are similar in size to carbon, and nitrogen atom doping can impart various improved physicochemical and structural properties to carbon-based materials, enhancing lithium adsorption capacity. Finally, the decomposition and release of N_2 from the lithium azide can prevent the growth of SnSb nanocrystals during heat treatment, so as to the SnSb alloy nanoparticles are homogeneous distributed inside the porous carbon nanofibers. Therefore, the SnSb@N-PCNFs display enhanced electrochemical performance. The SnSb@N-PCNFs electrode possesses a specific capacity of 1336 mA h g^{-1} at the first discharge cycle, and after 100 cycles the capacity can still be maintained at 892 mA h g^{-1} at 100 mA g^{-1} for LIBs. Furthermore, a reversible capacity of 487 mA h g^{-1} after 1000 cycles is presented at a high rate of 2000 mA g^{-1}, indicating the remarkable long-term cycling stability of SnSb@N-PCNFs electrode.

2. Experimental section

2.1. Materials synthesis

SnSb@N-PCNFs was synthesized through an electrospinning technique followed by stepwise thermal annealing processes. In a typical synthesis, polyacrylonitrile (PAN, 0.4g, Sigma-Aldrich, Mw = 150,000) and polyvinyl-pyrrolidone (PVP, 0.4g, Sigma-Aldrich, Mw = 1,300,000) were mixed with N,*N*-dimethylformamide (DMF, 10 mL) at 80 °C Stirred for 24 h to form PAN/PVP solution. Subsequently, $SnCl_2 \cdot 2H_2O$ (97%, 2.5 mmol) and $SbCl_3$ (98%, 2.5 mmol), lithium azide (LiN_3, 16% in term of PAN/PVP weight) were completely dissolved in the PAN/PVP solution, stirring for 6 h, the resultant solution was used as the precursor for electrospinning, and the flow rate was controlled to be 0.2 mL h^{-1}, the distance between the needle and the collector is about 15 cm. Electrospinning was initiated by supplying a voltage of 16 kV.

The as-spun nanofibers were first dissolvent for 24 h. Next, the nanofibers were heated to 120 °C and stabilized for 30 min, followed by heating to 240 °C for 120 min at a heating rate of 0.5 °C min^{-1}, then heating to 600 °C for 3 h with a heating rate of 2 °C min^{-1}. For comparison, SnSb@N-PCNFs is prepared with different lithium azide content (8%, 24%) and different carbonization temperature (500 °C, 700 °C), but the other conditions are constant, so as to study the best conditions for uniform distribution of SnSb nanoparticles in N-doped porous carbon nanofibers. In addition, SnSb/CNFs was also fabricated using the same synthetic conditions, except that no LiN3 was added into the precursors solution for electrospinning.

2.2. Materials characterization

The composition of the powdery was studied by XRD with Cu Kα radiation. The JEOL 7500FA TEM and JEOL 2011F FE-SEM were used to investigate the microstructures of the as-synthesized samples. Thermogravimetric analysis (TG, STA 409 C) of the samples was investigated under air. XPS, Raman spectra and nitrogen absorption/desorption isotherms (BET technique) were obtained by a Perkin Elmer PHI 5000C ESCA XPS system, NEXUS 670 FT-IR Raman spectrometer and NOVA 4200e instrument.

2.3. Electrochemical measurements

Electrochemical measurements were performed using coin type 2032 cells. The active materials (SnSb@N-PCNFs, SnSb/CNFs), carbon black and PVDF were mixed in NMP with a weight ratio of 8: 1: 1. The solid loading in the electrode is about 1 mg. The electrolyte consisted of a mixture of 1 M $LiPF_6$ in ethylene carbonate/dimethyl carbonate (1:1 by volume). The galvanostatic charge/discharge performances were performed on a LAND-CT2001C test system with the range of 0.001–3 V (vs Li/Li^+). Cyclic voltammogram (CV) curves and electrochemical impedance spectra (EIS) analysis were performed using an electrochemical workstation.

3. Results and discussion

The synthesis process of the SnSb@N-PCNFs is schematically demonstrated in Fig. 1. In a typical procedure, a precursor composed of Polyacrylonitrile (PAN), polyvinyl-pyrrolidone (PVP), lithium azide (LiN_3), $SnCl_2$, and $SbCl_3$ in N,*N*-dimethylformamide (DMF) was prepared and electrospun on a copper foil. After desolvent for 24 h, in which LiN_3, $SnCl_2$ and $SbCl_3$ tend to accumulate inside the PAN/PVP nanofibers because of the phase separation during drying process, the fibers were carbonized under N_2 to synthesize CNFs. During the carbonization process, when heated to 240 °C, lithium azide will simultaneously undergo a severe decomposition process, forming a large amount of Li_3N and N_2, eventually forming a rich mesopores inside the nanofibers. With the increase of the carbonization temperature, it functions as a separator to prevent the agglomeration of SnSb nanoparticles and inhibit their growth into larger particles.

The scanning electron microscopy (SEM) image shows the as-spun (Fig. 2a–c) and carbonized (Fig. 2d–f) nanofibers with different LiN_3 concentration. The as-spun nanofibers present an average diameter about 220 nm. However, with the addition of different LiN_3 content, the morphology of the carbon nanofibers obtained under the same calcination process varies greatly. For the sample without the addition of lithium azide, it can be seen that most of nanoparticles grow on the surface of the fiber, and the average diameter is about 200 nm (Fig. 2d), with the product expressed as SnSb/CNFs. When the content of lithium azide was increased to 8%, some particles are presented on the surface of the fiber, and the average diameter of the fiber is reduced to about 180 nm (Fig. 2e). When the lithium azide content is further

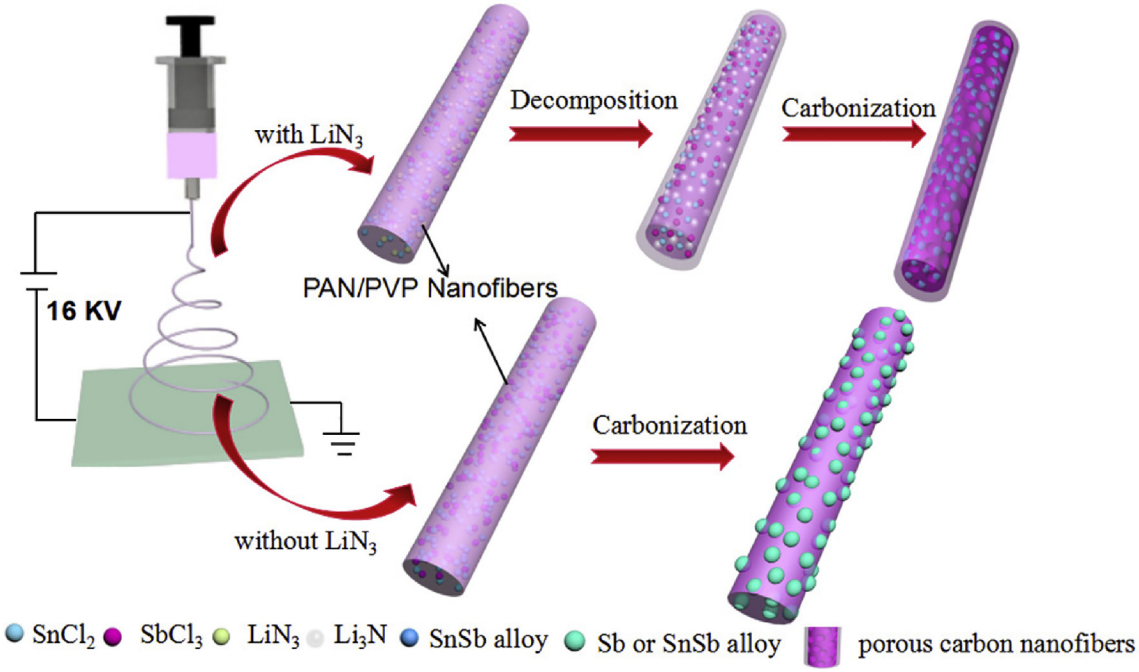

Fig. 1. Schematic illustration of the fabrication process of SnSb@N-PCNFs composites.

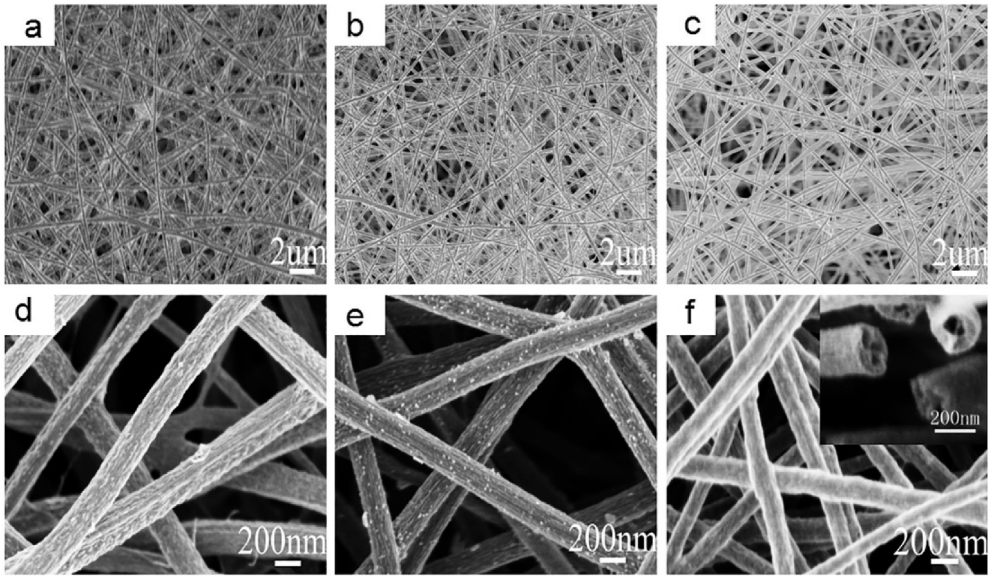

Fig. 2. SEM images of as-spun $SnCl_2/SbCl_3$/PAN/PVP nanofibers with different LiN_3 concentrations of (a) 0%, (b) 8%, (c) 16%; SEM images of (d) SnSb/CNFs, (e) SnSb@N-PCNFs with 8% LiN_3, (f) SnSb@N-PCNFs with 16% LiN_3 corresponding to (a–c) after annealed at 600 °C in N_2. (Inset: the cross section (f) of SnSb@N-PCNFs)

increased to 16%, no SnSb nanoparticles are found on the surface of the fibers (Fig. 2f), suggesting all SnSb nanoparticles have been encapsulated inside the carbon nanofibers. It can be seen that the surface of the fiber is very rough, which is also conducive to the diffusion of lithium ions from different directions, thereby ameliorating the electrochemical performance of the material. The inset of Fig. 2f shows a magnified cross section of SnSb@N-PCNFs, in which the porous interior structure of these fibers was revealed. When the lithium azide content was increased to 24%, the precursor nanofibers obtained by electrospinning appeared agglomeration (Fig. S1, Supporting Information), indicating that the suitable addition content of lithium azide content is 16% in this study.

The TEM images of SnSb/CNFs and SnSb@N-PCNFs are shown in Fig. 3. It can be clearly observed that under the same calcination procedure, for the sample without the addition of lithium azide, no porous structure can be observed and most of the metal nanoparticles are grown on the surface of CNFs (Fig. 3a). When the content of lithium azide is 8%, A large number of SnSb alloy nanoparticles are still observed on the surface of the CNFs, and the porous structure inside the fiber is not obvious (Fig. 3b), in accordance with the SEM results (Fig. 2d and e). Further increasing the lithium azide to 16%, clear porous structure for the CNFs is observed, and the majority of SnSb alloy nanoparticles is embedded

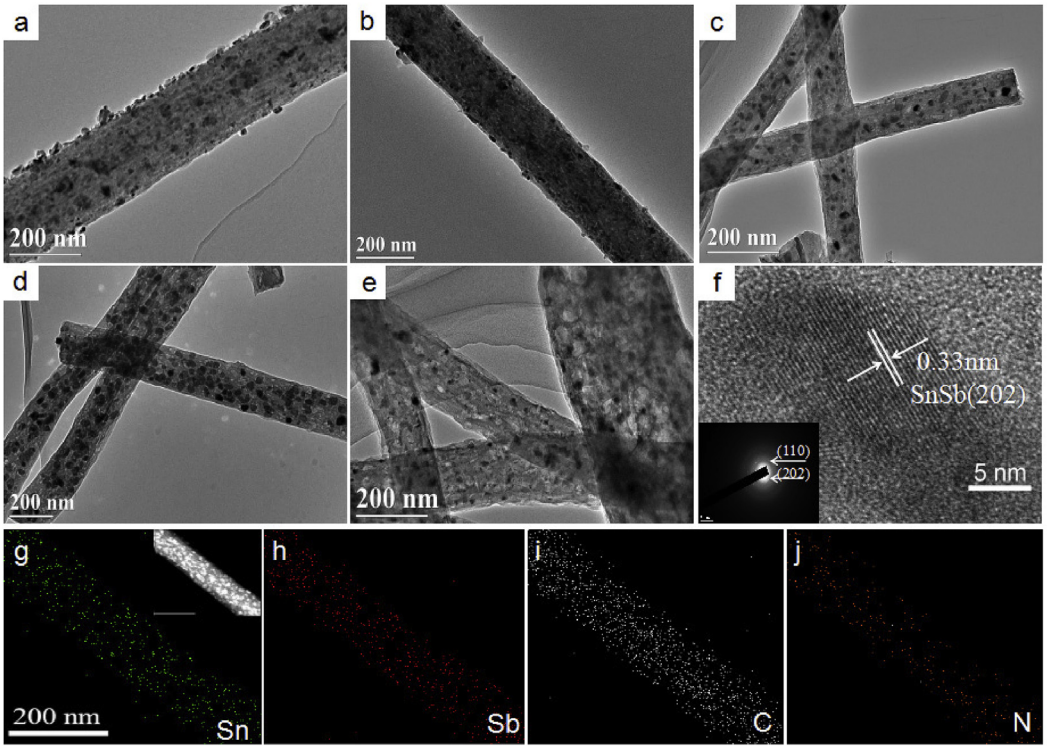

Fig. 3. TEM images of (a) SnSb/CNFs without LiN_3, (b) SnSb@N-PCNFs with 8% LiN_3. TEM images of SnSb@N-PCNFs with 16% LiN_3 treated by carbonization at (c) 500 °C and (d) 700 °C. TEM images(e) and HRTEM image (f) of SnSb@N-PCNFs with 16% LiN_3 treated by carbonization at 600 °C. The inset of panel (f) shows the corresponding SAED patterns. (g–j) Elemental mapping of SnSb@N-PCNFs.

in the CNFs (Fig. 3e). These results highlight that the proper LiN_3 content can not only produce mesopores in the carbon nanofibers but also prevent the growth of the metal nanoparticles on the surface of the CNFs during the carbonization process [42]. Moreover, the optimum carbonization temperature during the synthesis of SnSb@N-PCNFs is important for the pore filling effect inside the fiber and the inhibition of the aggregation and their growth of SnSb nanoparticles [38]. With the same lithium azide content (16%), when the carbonization temperature is 500 °C, the size and distribution of SnSb nanoparticles inside the fibers are not uniform (Fig. 3c). When the temperature is raised to 700 °C, the SnSb nanoparticles are aggregated, and the particle diameter is increased to about 30 nm (Fig. 3d, Fig. S8). Fig. 3e shows the TEM images of SnSb@N-PCNFs prepared at a carbonization temperature of 600 °C. It verifies that the abundant of mesopores generated during calcination and distributed inside the CNFs, and the SnSb alloy particles with a particle size of 12–20 nm are evenly distributed inside the porous CNFs (Fig. S2). Clearly, the best morphology of SnSb@N-PCNFs is obtained when the content of LiN_3 is 16% and the carbonization temperature is 600 °C. In this regard, the SnSb@N-PCNFs mentioned below are all prepared under this condition.

The HRTEM image of SnSb@N-PCNFs displays clear lattice fringes for SnSb alloy nanoparticles (Fig. 3f), and the interplanar spacing of the nanoparticle is 0.33 nm, which corresponds to the (202) planes of the SnSb alloy. No significant carbon lattice fringes were noticed, demonstrating the amorphous nature of carbon [43,44]. SAED patterns (inset of Fig. 3f) show dispersing diffraction rings, further describing the crystalline character of SnSb alloy nanoparticles, which agrees well with the XRD results (Fig. 4a). Energy dispersive X-ray spectroscopy elemental mapping (Fig. 3g–j) shows that the Sn, Sb, C and N atoms are homogeneously scattered in the as-prepared SnSb@N-PCNFs. These results indicate that LiN_3 can be used as a punching agent, and also as N source to form N-doped porous carbon nanofibers. The structure of SnSb@N-PCNFs was studied by nitrogen adsorption/desorption isotherm as shown in Fig. S3. The surface area of 160.24 $m^2 g^{-1}$ is revealed on the basis of the BET method. The pore sizes of SnSb@N-PCNFs (the inset of Fig. S3) are essentially distributed between 2 and 50 nm, which affirms the porous nature of the SnSb@N-PCNFs, corresponds well with the SEM/TEM results. The presence of abundant porous structure will promote the rapid access of the interaction between Li-ions and active materials, enable easy to access with electrolyte, and buffer the volume change in the process of repeated charge and discharge [38,45].

The as-prepared SnSb@N-PCNFs was further studied by XRD. It can be seen from Fig. 4a that all sharp diffraction peaks of SnSb@N-PCNFs can be well indexed to (101), (110), (021), (202), (211) and (122) crystal planes of the SnSb alloy (JCPDS No. 33–0118), indicting the high crystallinity and phase purity of the SnSb alloy in the SnSb@N-PCNFs [46]. In fact, even carbonization at a lower temperature of 500 °C, the XRD test results also show that all the diffraction peaks correspond to pure SnSb alloy phase (JCPDS No. 33–0118) (Fig. S4). However, for the SnSb/CNFs without LiN_3, which was treated by carbonization at 600 °C, two weak diffraction peaks corresponding to the Sb phase are appeared in the XRD patterns [47]. These results confirm that the addition of lithium azide can effectively promote the SnSb alloying reaction.

The Raman spectrum of SnSb@N-PCNFs (Fig. 4b) displays typical D band (1360 cm^{-1}) and G band (1592 cm^{-1}). The relative strength between D and G bands is commonly used to indicate the integrity and graphitization of carbon materials. For the SnSb@N-PCNFs, the I_D/I_G value is about 0.87, which is the same as the TEM results [38]. The formation of abundant defects in the N-doped porous carbon nanofiber can promote the diffusion of lithium ions, and provide more insertion sites for lithium storage, are helpful for the improvement of the overall capacity of the SnSb@N-PCNFs [45,47].

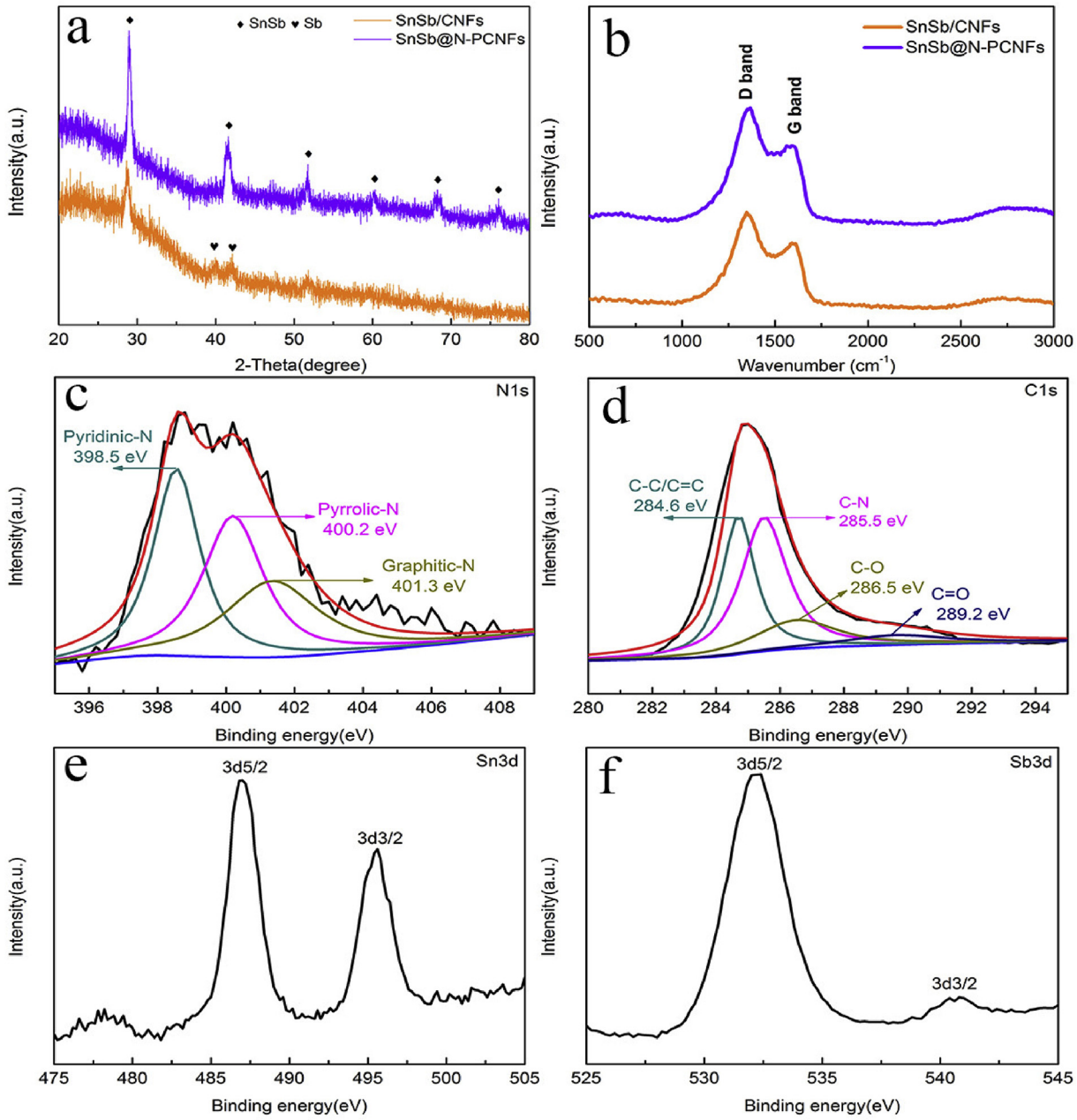

Fig. 4. (a) XRD patterns and (b) Raman spectra of SnSb@N-PCNFs and SnSb/CNFs. High-resolution (c) N 1s, (d) C 1s, Sn3d (e) and Sb3d (f) XPS spectra of the SnSb@N-PCNFs.

The content of carbon in the SnSb@N-PCNFs was confirmed to be 44.8% by weight loss on the basis of the thermogravimetric analysis (TGA) results (Fig. S5a). It must be noted that the weight reduction of SnSb@N-PCNFs between 170 °C and 240 °C is mainly attributed to the decomposition of LiN_3. XPS analyses were performed to further clarify the chemical compositions of the products. In the full XPS survey spectra (Fig. S5b), the C, N, Sn and Sb can be clearly observed [31]. In particular, the N1s spectrum (Fig. 4c) could be divided into three subpeaks and the nitrogen content was confirmed to be 5.8 wt %, which is ascribed to the reaction between CNFs and Li_3N and which is produced by the decomposition of LiN_3 during the carbonization process. Besides, the C1s XPS profile (Fig. 4d) further verified the formation of C-N bonds (285.5 eV). The characteristic peaks of Sn and Sb were further investigated by XPS analysis (Fig. 4e and f). The two peaks were owing to the $3d_{5/2}$ and $3d_{3/2}$ orbitals of Sn and Sb, respectively, which confirmed the formation of the SnSb nanoparticles inside the N-PCNFs. These results indicate that the strategy for the synthesis of SnSb@N-PCNFs is versatile and efficient, and the synthesized SnSb@N-PCNFs own several main superiority to achieve advanced electrochemical performance, such as homogeneous particle size and uniform distribution of SnSb alloy nanoparticles, as well as porous structures.

Fig. 5 presented the electrochemical performance of SnSb@N-PCNFs as anode material for LIBs. The cyclic voltammograms of the initial five cycles for SnSb@N-PCNFs (Fig. 5a) were collected at a scan rate of 0.2 mV s^{-1} between 0.001 and 3 V. The wide reduction peak appeared in the range of 1.8 to 0.9 V in the initial cathodic scan, and vanished in the subsequent scan, implying the formation of solid electrolyte interphase (SEI) film [16,48]. It can also be clearly seen that there are two reduction peaks at around 0.75 and

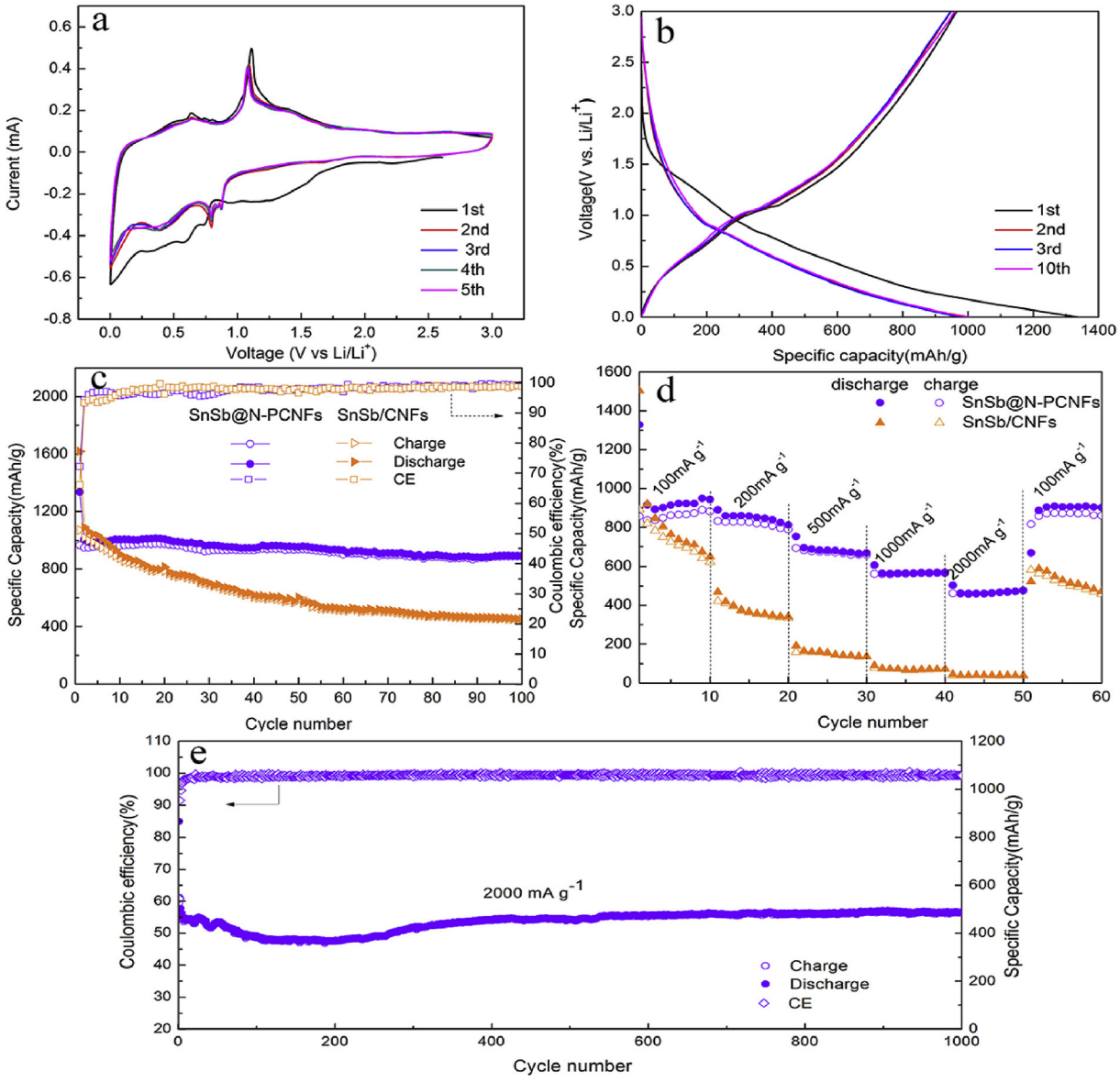

Fig. 5. Electrochemical performance of the SnSb@N-PCNFs electrode in LIBs. a) Cyclic voltammograms for the initial five cycles of the SnSb@N-PCNFs electrode at a scanning rate of 0.2 mV s^{-1} b) Galvanostatic discharge–charge profiles for selected cycles at a current density of 100 mA g^{-1} c) Cycling performance at a current density of 100 mA g^{-1} and Coulombic efficiency of SnSb@N-PCNFs electrode, with SnSb/CNFs included for comparison. d) Rate performance at different current densities from 100 to 2000 mA g^{-1}, with SnSb@CNFs included for comparison. e) Cycling performance at a current density of 2000 mA g^{-1}.

0.4 V corresponding to the formation of the Li_3Sb and $Li_{4.4}Sn$, respectively. The electrochemical reaction is as follows: SnSb → Li_3Sb + Sn → Li_3Sb + $Li_{4.4}Sn$. It can be seen from the first anodic scan that the two oxidation peaks are around 0.6–0.8 V and 1.1 V, which corresponds to the dealloying reactions of the $Li_{4.4}Sn$ and Li_3Sb, with the charge process: Li_3Sb + $Li_{4.4}Sn$ → Li_3Sb + Sn → Sb + Sn. The subsequent four cycles are almost overlapped, indicating that the SnSb@N-PCNFs electrode materials present good electrochemical reversibility [46]. Fig. 5b shows the galvanostatic discharge–charge profiles of SnSb@N-PCNFs at 100 mA g^{-1}, all voltage plateaus on the first charge-discharge curve corresponding to the peaks of the CV curve. In addition, it should be pointed out that the first discharge and charge capacity of the electrode was 1336 and 965 mA h g^{-1}, displaying a high initial Coulombic efficiency (CE) of 72.22%. The CE value is generally considered to be relatively high, indicating that the encapsulation of SnSb nanoparticles within the porous carbon nanofibers can significantly reduce the deleterious reaction between SnSb and electrolyte. The capacity loss of the first charge and discharge cycle is mainly due to the irreversible lithium loss caused by the formation of the SEI layer. By comparison, SnSb/CNFs electrodes can only provide a capacity of 1618 and 1070 mA h g^{-1} at 100 mA g^{-1} in the initial discharging–charging process, with a CE only of 66.13% (Fig. S6).

The SnSb@N-PCNFs electrode can provide a stable reversible capacity of 892.6 mA h g^{-1} after 100 cycles at 100 mA g^{-1} (Fig. 5c), while for SnSb/CNFs, after 100 cycles, a decreased capacity of 454.6 mA h g^{-1} is observed at 100 mA g^{-1}. Therefore, the SnSb@N-PCNFs electrode shows significant improvement in cycling stability. The rapid capacity fading for the SnSb/CNFs composite electrode after 20 cycles could be due to the separation and comminution of large size SnSb nanoparticles. The SnSb@N-PCNFs electrode shows evidently higher rate capacities than the SnSb/

CNFs electrode under all traditional current densities from 100 to 2000 mA g^{-1} (Fig. 5d). The capacity of SnSb@N-PCNFs electrode could still reach to 568 and 477 mA h g^{-1}, when the current density is increased to 1000 and 2000 mA g^{-1}. More importantly, when it reduced back to 100 mA g^{-1}, a capacity of 901 mA h g^{-1} can be stably provided. In contrast, the capacities of SnSb/CNFs electrode decreased to only 39 mA h g^{-1} at 2000 mA g^{-1}. It indicates that the strong tolerance of SnSb@N-PCNFs toward rapid lithium-ion insertion/extraction and further confirms the excellent cycling stability of the SnSb@N-PCNFs anode. Moreover, the high reversible capacity of 487 mA h g^{-1} can still be maintained after 1000 cycles at 2000 mA g^{-1} (Fig. 5e), significant improvement compared with previously reported results for SnSb-based materials.

To further illuminate the excellent electrochemical performance of SnSb@N-PCNFs electrode, the morphological changes of the SnSb@N-PCNFs electrode after the 200 charge/discharge cycles at 2000 mA g^{-1} were tested by TEM (Fig. 6a and b). The porous structure of SnSb@N-PCNFs is well maintained after 200 cycles, which illustrate that the nanostructure of the SnSb@N-PCNFs can effectively inhibit the pulverization and aggregation of SnSb nanoparticles in the process of repeated lithiation and delithiation, thereby insuring high cycling stability. Meanwhile, the EIS tests on the electrodes of SnSb@N-PCNFs and SnSb/CNFs were also tested before and after 100 cycles to gain a more in-depth understanding of the astonishing enhanced cycling performance of SnSb@N-PCNFs. As shown in Fig. S7, all Nyquist points exhibit a semicircular in the intermediate frequency region, this is related to the internal resistance in the electrode. Obviously, the charge transfer resistance of SnSb@N-PCNFs is much lower than that of SnSb/CNFs, representing that the electrochemical kinetics and conductivity of the entire electrode are highly enhanced. What's more, the semicircular diameter of SnSb@N-PCNFs does not increase too much even after 100 cycles at high frequency, indicating that the electrode surface forms a stable SEI laye during the first cycle, and this SEI layer maintains a good structural integrity.

Compared with the previous literature (Table S1), the SnSb@N-PCNFs displayed outstanding electrochemical performance as LIBs anode material due to its unique structure features as schematized in Fig. 6c. First, during the charge-discharge process, nitrogen-doped porous carbon nanofibers can provide enough voids to alleviate volume change and aggregation of SnSb nanoparticles, which is in favor of maintaining the structure integrity of the electrode. Moreover, the average particle size of SnSb alloy nanoparticles is 16 nm, which can remarkably increase the availability of the active material and decrease the mechanical strain in the process of electrochemical reaction [38]. In addition, the continuous one-dimensional nitrogen-doped porous carbon nanofibers have significant advantages in enhancing the electrochemical performance of LIBs due to their short diffusion distance and better conductivity. Finally, by promoting the contact between the electrolyte and the pores, the 3D hierarchical porous structure offers a large contact area of electrode/electrolyte and short lithium-ion transport pathways, and further improves the electrochemical activity of SnSb nanoparticles inside the porous carbon nanofibers. All

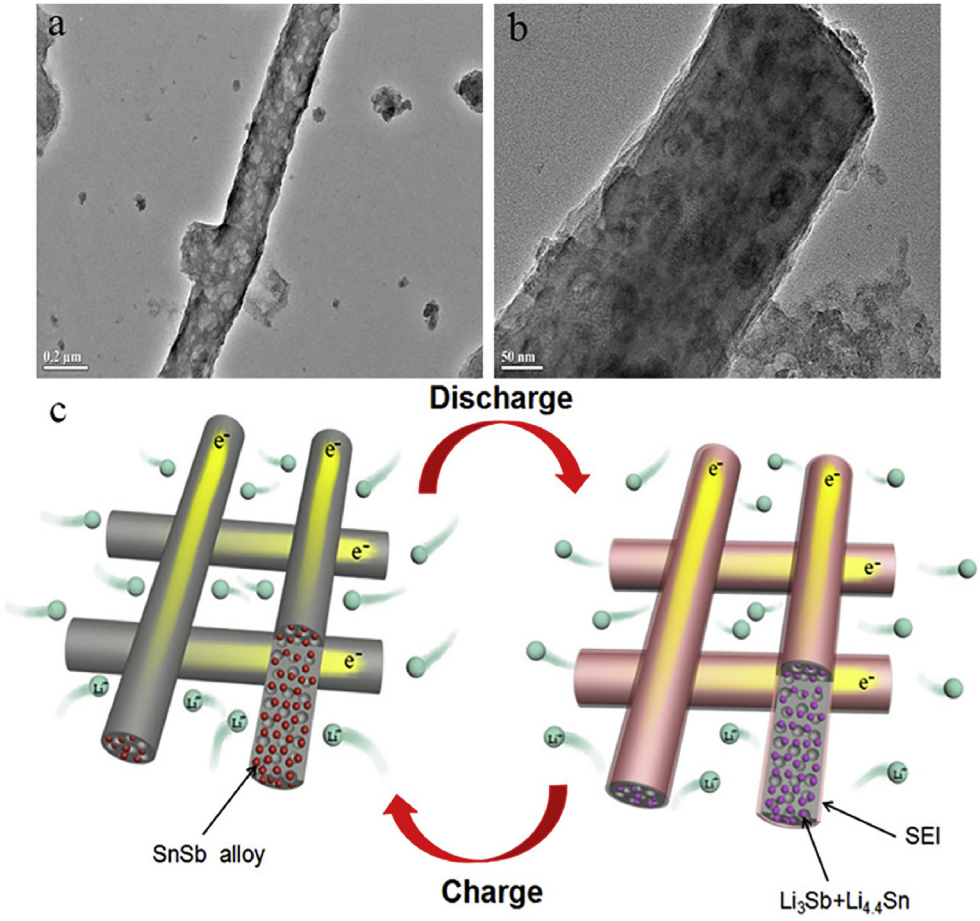

Fig. 6. (a, b) TEM images of SnSb@N-PCNFs after 200 discharge/charge cycles at 2000 mA g^{-1}. (c) Schematic illustration of the structural advantages of SnSb@N-PCNFs as anode materials.

these features are the main reasons for the high cycle performance of SnSb@N-PCNFs.

4. Conclusions

In summary, SnSb alloy nanoparticles were homogeneously embedded in N-doped porous carbon nanofibers, synthesized through a simple electrospinning technique. The employment of LiN_3 could not only paly as a porogen to produce a large amount of mesopores inside the nanofibers, but also inhibit particle aggregation and pulverization of the SnSb nanoparticles during long-term cycling process. This unique structure evidently increases the electrochemical performance of SnSb-based material as anode for LIBs. This study provides a new method for designing SnSb alloy as anode material for LIBs with high performance and stability, and this unique concept of synthesis can be also expanded to the preparation of various types of functional nanomaterials.

Acknowledgements

This work was partially supported by the National Key Research and Development Program of China (2017YFA0204600), the National Science Fund for Distinguished Young Scholars (51625102), the National Natural Science Foundation of China (51471053, 61704041, 61411136003), and the Science and Technology Commission of Shanghai Municipality (17XD1400700). Zhenguo Huang is grateful for the financial support from ARC (DP170101773).

Appendix A. Supplementary data

Supplementary data to this article can be found online at https://doi.org/10.1016/j.jallcom.2018.10.295.

References

[1] M. Li, J. Lu, Z. Chen, K. Amine, 30 Years of lithium-ion batteries, Adv. Mater. (2018) 1800561.
[2] P. Wang, M.X. Gao, H.G. Pan, J.L. Zhang, C. Liang, J.H. Wang, P. Zhou, Y.F. Liu, A facile synthesis of Fe_3O_4/C composite with high cycle stability as anode material for lithium-ion batteries, J. Power Sources 239 (2013) 466–474.
[3] Y. Lin, M.X. Gao, D. Zhu, Y.F. Liu, H.G. Pan, Effects of carbon coating and iron phosphides on the electrochemical properties of $LiFePO_4$/C, J. Power Sources 184 (2008) 444–448.
[4] D. Wang, M. Gao, H. Pan, J. Wang, Y. Liu, High performance amorphous-Si@SiOx/C composite anode materials for Li-ion batteries derived from ball-milling and in situ carbonization, J. Power Sources 256 (2014) 190–199.
[5] R. Hu, M. Zhu, H. Wang, J. Liu, O. Liuzhang, J. Zou, Sn buffered by shape memory effect of NiTi alloys as high-performance anodes for lithium ion batteries, Acta Mater. 60 (2012) 4695–4703.
[6] Y.F. Liu, H.G. Pan, M.X. Gao, Q.D. Wang, Advanced hydrogen storage alloys for Ni/MH rechargeable batteries, J. Mater. Chem. 21 (2011) 4743–4755.
[7] M. Gao, X. Chen, H. Pan, L. Xiang, F. Wu, Y. Liu, Ultrafine SnO_2 dispersed carbon matrix composites derived by a sol–gel method as anode materials for lithium ion batteries, Electrochim. Acta 55 (2010) 9067–9074.
[8] L. Liu, F. Xie, J. Lyu, T. Zhao, T. Li, B.G. Choi, Tin-based anode materials with well-designed architectures for next-generation lithium-ion batteries, J. Power Sources 321 (2016) 11–35.
[9] B. Liao, Y.Q. Lei, L.X. Chen, G.L. Lu, H.G. Pan, Q.D. Wang, A study on the structure and electrochemical properties of $La_2Mg(Ni_{0.95}M_{0.05})_9$ (M = Co, Mn, Fe, Al, Cu, Sn) hydrogen storage electrode alloys, J. Alloys Compd. 376 (2004) 186–195.
[10] H.G. Pan, Y.F. Liu, M.X. Gao, Y.Q. Lei, Q.D. Wang, A study of the structural and electrochemical properties of $La_{0.7}Mg_{0.3}(Ni_{0.85}Co_{0.15})_x$ (x=2.5-5.0) hydrogen storage alloys, J. Electrochem. Soc. 150 (2003). A 565-A 570.
[11] Z. Shen, Y. Hu, Y. Chen, X. Zhang, K. Wang, R. Chen, Tin nanoparticle-loaded porous carbon nanofiber composite anodes for high current lithium-ion batteries, J. Power Sources 278 (2015) 660–667.
[12] S.M. Zhang, H.T. Gu, H.G. Pan, S.H. Yang, W.B. Du, X. Li, M.X. Gao, Y.F. Liu, M. Zhu, L.Z. Ouyang, A novel strategy to suppress capacity and voltage fading of Li- and Mn-rich layered oxide cathode material for lithium-ion batteries, Adv. Energy Mater. 7 (2017), 1601066.
[13] Z. Yi, Q. Han, D. Geng, Y. Wu, Y. Cheng, L. Wang, One-pot chemical route for morphology-controllable fabrication of Sn-Sb micro/nano-structures: advanced anode materials for lithium and sodium storage, J. Power Sources 342 (2017) 861–871.
[14] D. Lakshmi, B. Nalini, P. Sivaraj, S. Jayapandi, Electro analytical studies on indium incorporated SnSb alloy anode for Li-ion batteries, J. Electroanal. Chem. 801 (2017) 459–465.
[15] G. Zhang, J. Zhu, W. Zeng, S. Hou, F. Gong, F. Li, C.C. Li, H. Duan, Tin quantum dots embedded in nitrogen-doped carbon nanofibers as excellent anode for lithium-ion batteries, Nano Energy 9 (2014) 61–70.
[16] M. He, M. Walter, K.V. Kravchyk, R. Erni, R. Widmer, M.V. Kovalenko, Monodisperse SnSb nanocrystals for Li-ion and Na-ion battery anodes: synergy and dissonance between Sn and Sb, Nanoscale 7 (2015) 455–459.
[17] X. Dong, W. Liu, X. Chen, J. Yan, N. Li, S. Shi, S. Zhang, X. Yang, Novel three dimensional hierarchical porous Sn-Ni alloys as anode for lithium ion batteries with long cycle life by pulse electrodeposition, Chem. Eng. J. 350 (2018) 791–798.
[18] P. Nithyadharseni, M.V. Reddy, B. Nalini, B.V.R. Chowdari, Electrochemical investigation of SnSb nano particles for lithium-ion batteries, Mater. Lett. 150 (2015) 24–27.
[19] L. Zhang, L. Lu, D. Zhang, W. Hu, N. Wang, B. Xu, Y. Li, H. Zeng, Dual-buffered SnSe@CNFs as negative electrode with outstanding lithium storage performance, Electrochim. Acta 209 (2016) 423–429.
[20] W. Fan, X. Liu, Z. Wang, P. Fei, R. Zhang, Y. Wang, C. Qin, W. Zhao, Y. Ding, Synergetic enhancement of the electronic/ionic conductivity of a Li-ion battery by fabrication of a carbon-coated nanoporous SnOxSb alloy anode, Nanoscale 10 (2018) 7605–7611.
[21] H. Wang, Q. Wu, D. Cao, X. Lu, J. Wang, M.K.H. Leung, S. Cheng, L. Lu, C. Niu, Synthesis of SnSb-embedded carbon-silica fibers via electrospinning: effect of TEOS on structural evolutions and electrochemical properties, Mater.i Today Energy 1–2 (2016) 24–32.
[22] X. Xia, Z. Li, H. Zhou, Y. Qiu, C. Zhang, The effect of deep cryogenic treatment on SnSb/C nanofibers anodes for Li-ion battery, Electrochim. Acta 222 (2016) 765–772.
[23] A.T. Tesfaye, Y.D. Yücel, M.K.S. Barr, L. Santinacci, F. Vacandio, F. Dumur, S. Maria, L. Monconduit, T. Djenizian, The electrochemical behavior of SnSb as an anode for Li-ion batteries studied by electrochemical impedance spectroscopy and electron microscopy, Electrochim. Acta 256 (2017) 155–161.
[24] X. Xia, Z. Li, L. Xue, Y. Qiu, C. Zhang, X. Zhang, The electrochemical performance of SnSb/C nanofibers with different morphologies and underlying mechanism, J. Mater. Res. 32 (2017) 1184–1193.
[25] P. Antitomaso, B. Fraisse, M.T. Sougrati, F. Morato-Lallemand, S. Biscaglia, D. Aymé-Perrot, P. Girard, L. Monconduit, Ultra-fast dry microwave preparation of SnSb used as negative electrode material for Li-ion batteries, J. Power Sources 325 (2016) 346–350.
[26] J. Choi, C. Ha, H. Choi, S. Lee, Carbon embedded SnSb composite tailored by carbothermal reduction process as high performance anode for sodium-ion batteries, J. Ind. Eng. Chem. 60 (2018) 451–457.
[27] Z. Li, J. Zhang, J. Shu, J. Chen, C. Gong, J. Guo, L. Yu, J. Zhang, Carbon nanofibers with highly dispersed tin and tin antimonide nanoparticles: preparation via electrospinning and application as the anode materials for lithium-ion batteries, J. Power Sources 381 (2018) 1–7.
[28] L. Li, K.H. Seng, D. Li, Y. Xia, H.K. Liu, Z. Guo, SnSb@carbon nanocable anchored on graphene sheets for sodium ion batteries, Nano Res. 7 (2014) 1466–1476.
[29] J. Kim, D. Kim, Synthesis of multiphase SnSb nanoparticles-on-SnO_2/Sn/C nanofibers for use in Li and Na ion battery electrodes, Electrochem. Commun. 46 (2014) 124–127.
[30] Z. Shen, Y. Hu, Y. Chen, R. Chen, X. He, X. Zhang, H. Shao, Y. Zhang, Controllable synthesis of carbon-coated Sn-SnO_2-carbon-nanofiber membrane as advanced binder-free anode for lithium-ion batteries, Electrochim. Acta 188 (2016) 661–670.
[31] L. Ji, M. Gu, Y. Shao, X. Li, M.H. Engelhard, B.W. Arey, W. Wang, Z. Nie, J. Xiao, C. Wang, J. Zhang, J. Liu, Controlling SEI formation on SnSb-porous carbon nanofibers for improved Na ion storage, Adv. Mater. 26 (2014) 2901–2908.
[32] C. Lin, L. Yang, L. Ouyang, J. Liu, H. Wang, M. Zhu, A new method for few-layer graphene preparation via plasma-assisted ball milling, J. Alloys Compd. 728 (2017) 578–584.
[33] L. Ouyang, Z. Cao, H. Wang, R. Hu, M. Zhu, Application of dielectric barrier discharge plasma-assisted milling in energy storage materials – a review, J. Alloys Compd. 691 (2017) 422–435.
[34] Q. Pan, F. Zheng, X. Ou, C. Yang, X. Xiong, M. Liu, MoS_2 encapsulated SnO_2 -SnS/C nanosheets as a high performance anode material for lithium ion batteries, Chem. Eng. J. 316 (2017) 393–400.
[35] Y. Wu, Q. Pan, F. Zheng, X. Ou, C. Yang, X. Xiong, M. Liu, D. Hu, C. Huang, Sb@C/expanded graphite as high-performance anode material for lithium ion batteries, J. Alloys Compd. 744 (2018) 481–486.
[36] G. He, Y. Song, S. Chen, L. Wang, Porous carbon nanofiber mats from electrospun polyacrylonitrile/polymethylmethacrylate composite nanofibers for supercapacitor electrode materials, J. Mater. Sci. 53 (2018) 9721–9730.
[37] M. Wang, Z. Huang, F. Kang, K. Liang, Porous carbon nanofibers with narrow pore size distribution from electrospun phenolic resins, Mater. Lett. 65 (2011) 1875–1877.
[38] G. Xia, Q. Gao, D. Sun, X. Yu, Porous carbon nanofibers encapsulated with peapod-like hematite nanoparticles for high-rate and long-life battery anodes, Small 13 (2017) 1701561.
[39] J. Choi, C. Ha, H. Choi, J. Seong, C. Park, S. Lee, Porous carbon-free SnSb anodes for high-performance Na-ion batteries, J. Power Sources 386 (2018) 34–39.
[40] J. Zhu, C. Shang, Z. Wang, J. Zhang, Y. Liu, S. Gu, L. Zhou, H. Cheng, Y. Gu, Z. Lu,

SnS/SnSb@C nanofibers with enhanced cycling stability via vulcanization as an anode for sodium-ion batteries, ChemElectroChem 5 (2018) 1098–1104.
[41] Z. Shen, Y. Hu, Y. Chen, X. Zhang, K. Wang, R. Chen, Tin nanoparticle-loaded porous carbon nanofiber composite anodes for high current lithium-ion batteries, J. Power Sources 278 (2015) 660–667.
[42] G. Xia, L. Zhang, F. Fang, D. Sun, Z. Guo, H. Liu, X. Yu, General synthesis of transition metal oxide ultrafine nanoparticles embedded in hierarchically porous carbon nanofibers as advanced electrodes for lithium storage, Adv. Funct. Mater. 26 (2016) 6188–6196.
[43] A. Birrozzi, F. Maroni, R. Raccichini, R. Tossici, R. Marassi, F. Nobili, Enhanced stability of SnSb/graphene anode through alternative binder and electrolyte additive for lithium ion batteries application, J. Power Sources 294 (2015) 248–253.
[44] C. Chen, G. Li, J. Zhu, Y. Lu, M. Jiang, Y. Hu, Z. Shen, X. Zhang, In-situ formation of tin-antimony sulfide in nitrogen-sulfur Co-doped carbon nanofibers as high performance anode materials for sodium-ion batteries, Carbon 120 (2017) 380–391.
[45] L. Zhang, G. Xia, Y. Huang, C. Wei, Y. Yu, D. Sun, X. Yu, MnO quantum dots embedded in carbon nanotubes as excellent anode for lithium-ion batteries, Energy Storage Mater. 10 (2018) 160–167.
[46] Q. Pan, Y. Wu, F. Zheng, X. Ou, C. Yang, X. Xiong, M. Liu, Facile synthesis of M-Sb (M = Ni, Sn) alloy nanoparticles embedded in N-doped carbon nanosheets as high performance anode materials for lithium ion batteries, Chem. Eng. J. 348 (2018) 653–660.
[47] J. Qin, T. Wang, D. Liu, E. Liu, N. Zhao, C. Shi, F. He, L. Ma, C. He, A top-down strategy toward SnSb in-plane nanoconfined 3D N-doped porous graphene composite microspheres for high performance Na-ion battery anode, Adv. Mater. 30 (2018) 1704670.
[48] Y. Zhu, X. Han, Y. Xu, Y. Liu, S. Zheng, K. Xu, L. Hu, C. Wang, Electrospun Sb/C fibers for a stable and fast sodium-ion battery anode, ACS Nano 7 (2013) 6378–6386.